A Synoptic Climatology and Composite Analysis of the Alberta Clipper

BLAINE C. THOMAS

Meteorology Branch, U.S. Army White Sands Missile Range, White Sands Missile Range, New Mexico

JONATHAN E. MARTIN

Department of Atmospheric and Oceanic Sciences, University of Wisconsin—Madison, Madison, Wisconsin

(Manuscript received 27 July 2005, in final form 12 June 2006)

ABSTRACT

Surface and upper-air analyses from the ECMWF Tropical Ocean Global Atmosphere (TOGA) dataset are used to construct a climatology of 177 Alberta clippers over 15 boreal cold seasons (October–March) from 1986/87 to 2000/01. The Alberta clipper (hereafter simply clipper) occurs most frequently during December and January and substantially less frequently during October and March. These cyclones generally move southeastward from the lee of the Canadian Rockies toward or just north of Lake Superior before progressing eastward into southeastern Canada or the northeastern United States, with less than 10% of the cases in the climatology tracking south of the Great Lakes. Characteristics of the structure and evolution of clippers during a 36-h period leading up to departure of the cyclone from the lee of the Canadian Rockies and a 60-h period after departure as the cyclone traverses central and eastern North America are examined through composite analyses. Over the course of the predeparture period, a cyclone over the Gulf of Alaska approaches the west coast of North America, and through its interaction with the mountainous terrain of western North America spawns a surface lee trough, characterized by a thermal ridge at 850 hPa, to the east of the Canadian Rockies. This thermal ridge dampens considerably as the composite clipper moves into central North America away from the immediate lee of the Canadian Rockies. The composite clipper system evolves from a lee cyclone with its nonclassical thermal structure to a more classically structured midlatitude cyclone as it moves through central and eastern North America largely as a result of rotation of the low-level thermal gradient and the increasing westward tilt with height of the composite clipper over the last 36 h of the postdeparture period. The thermal gradient rotation is dynamically linked to convergence of the along-isentrope component of the **Q** vector and thus to the ascent that sustains the clipper and creates some of its characteristic sensible weather elements. Such dynamical forcing is a direct consequence of the persistent westward displacement of the 500-hPa vorticity maximum with respect to the composite clipper sea level pressure minimum that characterizes the postdeparture period.

1. Introduction

One of the most significant synoptic-scale winter weather phenomena affecting central North America is the Alberta clipper, defined in the *Glossary of Meteorology* (Glickman 2000) as "a low pressure system that is often fast moving, has low moisture content, and originates in western Canada (in or near Alberta province)." Clippers[1] develop in the lee of the Canadian Rockies, a region characterized by a relative maximum in cyclogenesis events (Petterssen 1956; Reitan 1974; Chung et al. 1976; Zishka and Smith 1980; Whittaker and Horn 1981; Nielsen and Dole 1992). After initial formation, Alberta clippers generally move southeastward into south-central Canada or the north-central United States, then progress eastward toward the east

Corresponding author address: Jonathan E. Martin, Dept. of Atmospheric and Oceanic Sciences, University of Wisconsin—Madison, 1225 W. Dayton St., Madison, WI 53706.
E-mail: jemarti1@wisc.edu

[1] The terms "Alberta clipper" and "clipper" will be used interchangeably during the course of this paper and highlight both the region of origin of such systems as well as their rapid movement, à la clipper ships.

DOI: 10.1175/WAF982.1

coast of North America (Hutchinson 1995). The clipper track represents one of the major storm tracks for winter-season cyclones in the Northern Hemisphere (Petterssen 1956; Reitan 1974; Zishka and Smith 1980; Hoskins and Hodges 2002).

Most of the previous literature discussing the structure and evolution of the Alberta clipper has focused on the formative, lee cyclogenesis stage of the clipper (Henry 1925; Hess and Wagner 1948; Newton 1956; McClain 1960; Bonner 1961). Based upon this collective work, Palmén and Newton (1969) developed a conceptual model describing the development and evolution of northern Rocky Mountain lee cyclones and lee troughs. In this conceptual model, formation of the lee cyclone is preceded by the landfall of a cyclone from the Pacific Ocean along the west coast of North America. The lower-tropospheric wind flow crossing the Rocky Mountains increases as the Pacific cyclone approaches the coast, resulting in the development of a lee trough. The trough generally remains fixed to the lee slopes of the mountains and broadens over time as air warmed by descent is advected eastward. The approach of an upper-level trough and its associated vorticity maximum produces cyclonic development within the lee trough. Palmén and Newton stated that the cyclone moves away from the lee of the Rocky Mountains when a cold front overtakes the lee trough, but more recent studies (e.g., Locatelli et al. 1989; Martin et al. 1990) have shown that movement of the lee cyclone away from the mountains is not dependent on such a circumstance.

Although lee troughing commonly occurs in association with cross-mountain flow in the lower troposphere, additional conditions are necessary for the development of a cyclone within the lee trough.[2] Lee cyclogenesis often takes place when a region of strong ascent in the middle and upper troposphere associated with differential cyclonic vorticity advection is superimposed over a band of maximum descent in the lower troposphere (Newton 1956; Steenburgh and Mass 1994; Schultz and Doswell 2000). The resulting differential vertical motion generates cyclonic vorticity via column stretching. Differential cyclonic vorticity advection over an established low-level baroclinic zone in the lee of the Rockies also promotes the development of the lee cyclone (Steenburgh and Mass 1994; Davis 1997).

Within the spectrum of extratropical cyclones, Alberta clippers are generally regarded as rather innocuous, small-scale systems. Their characteristic lack of available moisture and rapid movement conspire to produce relatively low precipitation amounts over a narrow path. Moderate precipitation generally occurs in areas up to a few hundred kilometers north of the system's track while lighter precipitation generally falls to the south of the track (Harms 1973; Beckman 1987; Hutchinson 1995). Relatively little moisture is necessary, however, for clippers to produce snow accumulations of 80–150 mm (3–6 in.) in 3–6 h given the very cold air and correspondingly large snow-to-liquid equivalent ratios (generally 20 to 1 or greater) associated with these systems (Harms 1973). Snowfall amounts can be enhanced through an influx of low-level moisture from the Great Lakes into the clipper (Harms 1973; Vinzani and Changnon 1981; Silberberg 1990, Angel and Isard 1997) or as a result of locally intense upper-level forcing in the presence of low conditional stability (either potential or symmetric) (Smart and Carr 1986; Silberberg 1990; Gallus and Bresch 1997).

Often the most significant sensible weather element associated with Alberta clippers is strong wind. Areas in the lee of the Rocky Mountains and Alberta are susceptible to frontal chinooks as a Pacific cyclone approaches the British Columbia coast and the Alberta clipper develops within the lee trough (Price 1971; Oard 1993; Schultz and Doswell 2000). Over central and eastern North America, the strongest winds are usually located on the western side of the Alberta clipper in the region between the surface cyclone and the often-intense anticyclone trailing the clipper. Strong winds with clippers can also arise from enhanced isallobaric winds associated with a substantial pressure rise–fall couplet, and a downward transport of high-momentum air in regions of strong cold-air advection and low static stability (Kapela et al. 1995; Schultz and Doswell 2000). The strong winds that follow the passage of a clipper, coupled with preexisting or freshly fallen snow, can result in considerable blowing and drifting of snow and the creation of ground blizzard conditions (Stewart et al. 1995; Schwartz and Schmidlin 2002) and may, in the wake of a clipper passage, occasionally contribute to lake-effect snows along the southern and eastern shores of the Great Lakes.

Despite the acknowledged importance of the Alberta clipper to the wintertime weather of central North America, few studies have considered the synoptic-scale structure and evolution of these disturbances beyond the cyclogenesis stage. Furthermore, nearly every study that has examined these systems beyond the cyclogenesis stage has employed a case study approach. This paper examines the synoptic climatology of the Alberta clipper by considering its composite structure and evolution throughout the clipper life cycle. The paper is organized in the following manner. Section 2

[2] Pierrehumbert (1986) and Tibaldi et al. (1990) emphasize that lee troughing is not synonymous with lee cyclogenesis.

contains a description of the dataset and analysis method used to construct a synoptic climatology of Alberta clippers. Section 3 discusses the frequency, propagation, and sea level pressure characteristics of these cyclones. An analysis of the composite structure and evolution of Alberta clippers derived from all cases in the climatology is presented in section 4. An examination of the quasigeostrophic (QG) forcing for ascent throughout the clipper life cycle is presented in section 5, followed by discussion and conclusions in section 6.

2. Data and methodology

The climatology presented here was constructed using the European Centre for Medium-Range Weather Forecasts (ECMWF) Tropical Ocean Global Atmosphere (TOGA) surface and upper-air analyses for 15 boreal cold seasons (October–March) from 1986/87 to 2000/01. The ECMWF TOGA dataset consists of twice-daily (0000 and 1200 UTC) sea level and 14 (15, starting January 1992; 21, starting April 1999) unequally spaced pressure level analyses with 2.5° latitude–longitude grid spacing on a global domain. These data are directly interpolated from the ECMWF operational, full-resolution surface and pressure level data.[3] The data were acquired from the National Center for Atmospheric Research in gridded binary format, then converted and transferred to General Meteorological Package (GEMPAK; desJardins et al. 1991) grids with a cylindrical equidistant grid projection. The GEMPAK grids were then accessed by FORTRAN 77 programs for the purposes of performing diagnostic computations using sea level pressure (SLP), geopotential height, temperature, and the zonal and meridional components of the wind. Use of the ECMWF analyses was motivated both by computational convenience as well as availability at the commencement of the research. The resolution of these data is sufficient to identify Alberta clippers since the typical clipper is ~15° (six grid points) in diameter.

For this study, a cyclone qualified as an Alberta clipper if all of the following criteria were met.

1) The cyclone originated in the lee of the Canadian Rockies in Alberta, northeastern British Columbia, or far southwestern Northwest Territories.
2) The cyclone was defined by at least one closed isobar (analyzed at 2-hPa intervals) and/or a distinct local minimum in a SLP trough for at least 60 h following its departure from the Canadian Rockies. The time of departure, adapted from Schultz and Doswell (2000), is defined as the last analysis time before the SLP minimum begins making appreciable movement away from the Canadian Rockies.
3) The SLP minimum progressed southeastward from its region of origin to south-central Canada or the north-central United States, and then continued eastward (e.g., adapted from Hutchinson 1995).
4) The surface cyclone had an association with a migratory 500-hPa vorticity maximum (e.g., adapted from Hutchinson 1995).
5) The SLP minimum moved east of 90°W within 60 h of departure from the Canadian Rockies. This criterion excluded from the climatology cyclones that had short trajectories or exceptionally slow movement, characteristics common to about one-quarter of all cyclones originating in the lee of the Canadian Rockies (Chung et al. 1976).

A total of 177 cyclones satisfied all of the above criteria (Table 1).

3. Distribution of Alberta clippers

The cumulative monthly frequency of all clippers during the 15-season climatology is shown in Table 2. The larger number of cases observed during the middle of the cold season is a consequence of the more southerly position of the jet stream that provides a more favorable upper-level flow pattern for clipper development. Table 2 also demonstrates that clipper occurrence exhibits considerable intraseasonal and interannual variability.

a. Propagation characteristics

Figure 1 shows the track of each of the 177 Alberta clippers in the climatology from the time of departure to 60 h after departure. Tracks for each case were constructed by finding the position of the SLP minimum at each 12-h analysis time from departure to 60 h after departure and connecting the position points with straight lines. Most of the clippers moved southeastward toward or just north of Lake Superior before moving into southeastern Canada or New England, with only 15 of 177 cases tracking completely south of the Great Lakes. Some clippers moved at an especially fast rate (average speed of 13 m s^{-1}),[4] with 33 cases

[3] The operational resolution of the ECMWF model during the period of this climatology was T63 through 16 September 1991, T213 from 17 September 1991 through 31 March 1998, T_L319 from 1 April 1998 through 20 November 2000, and T_L511 from 21 November 2000 onward.

[4] This represents the speed of the fastest 20% of clippers. For comparison, the average speed of the rest of the clippers identified in this study was 9.7 m s^{-1}.

TABLE 1. Alberta clipper cases in the climatology. The time listed is the departure time for each case.

Time and date		
1200 UTC 20 Oct 1986	1200 UTC 20 Feb 1991	1200 UTC 25 Mar 1996
0000 UTC 2 Nov 1986	1200 UTC 4 Mar 1991	0000 UTC 12 Oct 1996
1200 UTC 13 Nov 1986	1200 UTC 7 Mar 1991	1200 UTC 8 Nov 1996
1200 UTC 15 Nov 1986	0000 UTC 20 Oct 1991	0000 UTC 20 Dec 1996
1200 UTC 1 Dec 1986	0000 UTC 20 Nov 1991	0000 UTC 31 Dec 1996
1200 UTC 4 Dec 1986	1200 UTC 25 Nov 1991	1200 UTC 1 Jan 1997
0000 UTC 6 Dec 1986	1200 UTC 4 Dec 1991	0000 UTC 14 Jan 1997
1200 UTC 7 Dec 1986	0000 UTC 6 Dec 1991	1200 UTC 30 Jan 1997
0000 UTC 10 Dec 1986	0000 UTC 25 Dec 1991	0000 UTC 31 Jan 1997
0000 UTC 30 Dec 1986	1200 UTC 13 Jan 1992	1200 UTC 12 Feb 1997
0000 UTC 18 Jan 1987	1200 UTC 18 Jan 1992	0000 UTC 15 Feb 1997
1200 UTC 20 Jan 1987	1200 UTC 21 Jan 1992	0000 UTC 17 Feb 1997
1200 UTC 1 Feb 1987	1200 UTC 24 Jan 1992	1200 UTC 21 Feb 1997
1200 UTC 6 Feb 1987	1200 UTC 28 Jan 1992	1200 UTC 24 Feb 1997
1200 UTC 25 Mar 1987	1200 UTC 4 Feb 1992	0000 UTC 20 Mar 1997
1200 UTC 7 Oct 1987	1200 UTC 19 Feb 1992	0000 UTC 23 Mar 1997
1200 UTC 28 Oct 1987	0000 UTC 27 Feb 1992	1200 UTC 25 Mar 1997
0000 UTC 10 Dec 1987	0000 UTC 19 Oct 1992	1200 UTC 26 Mar 1997
0000 UTC 21 Jan 1988	1200 UTC 26 Oct 1992	1200 UTC 28 Mar 1997
0000 UTC 23 Jan 1988	1200 UTC 15 Nov 1992	1200 UTC 30 Oct 1997
0000 UTC 8 Feb 1988	0000 UTC 9 Dec 1992	1200 UTC 17 Dec 1997
0000 UTC 29 Feb 1988	0000 UTC 24 Dec 1992	0000 UTC 27 Dec 1997
1200 UTC 30 Oct 1988	0000 UTC 27 Jan 1993	1200 UTC 29 Dec 1997
0000 UTC 2 Dec 1988	0000 UTC 6 Mar 1993	0000 UTC 31 Dec 1997
1200 UTC 13 Dec 1988	1200 UTC 8 Mar 1993	0000 UTC 30 Jan 1998
1200 UTC 29 Dec 1988	1200 UTC 18 Mar 1993	0000 UTC 8 Oct 1998
0000 UTC 16 Jan 1989	1200 UTC 9 Oct 1993	1200 UTC 13 Nov 1998
0000 UTC 17 Jan 1989	1200 UTC 22 Oct 1993	1200 UTC 15 Nov 1998
1200 UTC 18 Jan 1989	0000 UTC 27 Oct 1993	1200 UTC 24 Nov 1998
1200 UTC 21 Jan 1989	0000 UTC 3 Nov 1993	0000 UTC 8 Dec 1998
0000 UTC 23 Feb 1989	0000 UTC 20 Nov 1993	0000 UTC 17 Dec 1998
1200 UTC 10 Nov 1989	0000 UTC 18 Dec 1993	0000 UTC 30 Dec 1998
0000 UTC 16 Nov 1989	0000 UTC 20 Dec 1993	1200 UTC 2 Feb 1999
0000 UTC 19 Nov 1989	1200 UTC 27 Dec 1993	1200 UTC 7 Feb 1999
1200 UTC 21 Nov 1989	1200 UTC 30 Dec 1993	0000 UTC 23 Feb 1999
0000 UTC 24 Nov 1989	1200 UTC 22 Jan 1994	0000 UTC 19 Mar 1999
1200 UTC 28 Nov 1989	0000 UTC 5 Feb 1994	1200 UTC 3 Oct 1999
1200 UTC 30 Nov 1989	1200 UTC 13 Feb 1994	0000 UTC 17 Oct 1999
1200 UTC 8 Dec 1989	0000 UTC 13 Mar 1994	0000 UTC 24 Oct 1999
0000 UTC 12 Dec 1989	1200 UTC 25 Mar 1994	0000 UTC 8 Nov 1999
0000 UTC 24 Dec 1989	0000 UTC 23 Nov 1994	0000 UTC 25 Nov 1999
1200 UTC 4 Jan 1990	0000 UTC 1 Dec 1994	1200 UTC 28 Dec 1999
0000 UTC 6 Jan 1990	1200 UTC 8 Dec 1994	1200 UTC 29 Dec 1999
0000 UTC 10 Jan 1990	1200 UTC 26 Dec 1994	1200 UTC 30 Dec 1999
1200 UTC 18 Jan 1990	0000 UTC 9 Feb 1995	1200 UTC 4 Jan 2000
1200 UTC 20 Jan 1990	1200 UTC 15 Feb 1995	0000 UTC 7 Jan 2000
1200 UTC 22 Jan 1990	0000 UTC 21 Feb 1995	0000 UTC 21 Jan 2000
1200 UTC 5 Feb 1990	0000 UTC 2 Mar 1995	1200 UTC 1 Feb 2000
0000 UTC 8 Feb 1990	0000 UTC 18 Oct 1995	1200 UTC 18 Feb 2000
1200 UTC 22 Feb 1990	1200 UTC 11 Nov 1995	1200 UTC 13 Nov 2000
0000 UTC 5 Oct 1990	1200 UTC 21 Nov 1995	0000 UTC 27 Nov 2000
1200 UTC 21 Oct 1990	1200 UTC 29 Nov 1995	1200 UTC 6 Dec 2000
0000 UTC 31 Oct 1990	1200 UTC 1 Dec 1995	0000 UTC 19 Dec 2000
0000 UTC 24 Nov 1990	1200 UTC 12 Jan 1996	1200 UTC 27 Dec 2000
1200 UTC 6 Dec 1990	0000 UTC 16 Jan 1996	0000 UTC 1 Jan 2001
1200 UTC 23 Dec 1990	0000 UTC 6 Feb 1996	0000 UTC 4 Jan 2001
1200 UTC 12 Jan 1991	0000 UTC 9 Feb 1996	1200 UTC 5 Jan 2001
1200 UTC 18 Jan 1991	1200 UTC 13 Feb 1996	0000 UTC 3 Feb 2001
1200 UTC 21 Jan 1991	0000 UTC 15 Mar 1996	0000 UTC 21 Feb 2001

TABLE 2. The number of Alberta clippers that developed during each individual month and year in the climatology. Boldface numbers represent monthly totals. Numbers in parentheses indicate the number of Alberta clippers normalized to a 30-day month for each of the months.

Season	Oct	Nov	Dec	Jan	Feb	Mar	Total
1986/87	1	3	6	2	2	1	15
1987/88	2	0	1	2	2	0	7
1988/89	1	0	3	4	1	0	9
1989/90	0	7	3	6	3	0	19
1990/91	3	1	2	3	1	2	12
1991/92	1	2	3	5	3	0	14
1992/93	2	1	2	1	0	3	9
1993/94	3	2	4	1	2	2	14
1994/95	0	1	3	0	3	1	8
1995/96	1	3	1	2	3	2	12
1996/97	1	1	2	4	5	5	18
1997/98	1	0	4	1	0	0	6
1998/99	1	3	3	0	3	1	11
1999/2000	3	2	3	3	2	0	13
2000/01	0	2	3	3	2	0	10
Total	**20** (19.4)	**28** (28.0)	**43** (41.6)	**37** (35.8)	**32** (34.0)	**17** (16.5)	177

reaching the east coast of North America within 60 h of departure.

b. Sea level pressure characteristics of clippers

Though use of SLP as a measure of cyclone intensity is susceptible to a number of potential shortcomings (Sinclair 1994, 1997; Mesinger and Treadon 1995; Pauley 1998), these are offset by the ease of access to SLP data in the ECMWF dataset and the ability to compare results from this study with other climatological studies that have used SLP to assess cyclone strength in regions traversed by clippers (e.g., Hurley 1954; Harman et al. 1980; Angel and Isard 1998). Central SLP is therefore employed as a proxy measure of cyclone intensity.

Following the lead of numerous other studies (e.g., Sanders and Gyakum 1980; Roebber 1989; Nielsen and Dole 1992; Angel and Isard 1997), cyclone intensification is appraised by examining the SLP tendency calculated for each 12-h period from the time of departure ($T = 0$ h) to 60 h after departure ($T + 60$ h). Following Roebber (1989), the SLP tendencies were adjusted by latitude using the formula $\Delta P_{\text{adj}} = \Delta P(\sin \phi_{\text{ref}}/\sin \phi)$, where ΔP_{adj} is the adjusted SLP tendency, ΔP is the SLP tendency, ϕ_{ref} is a reference latitude of 50°N, and ϕ is the mean latitude of the clipper during the 12-h period. This adjustment to a reference latitude takes into account the fact that cyclones at different latitudes with similar pressure gradients will produce different

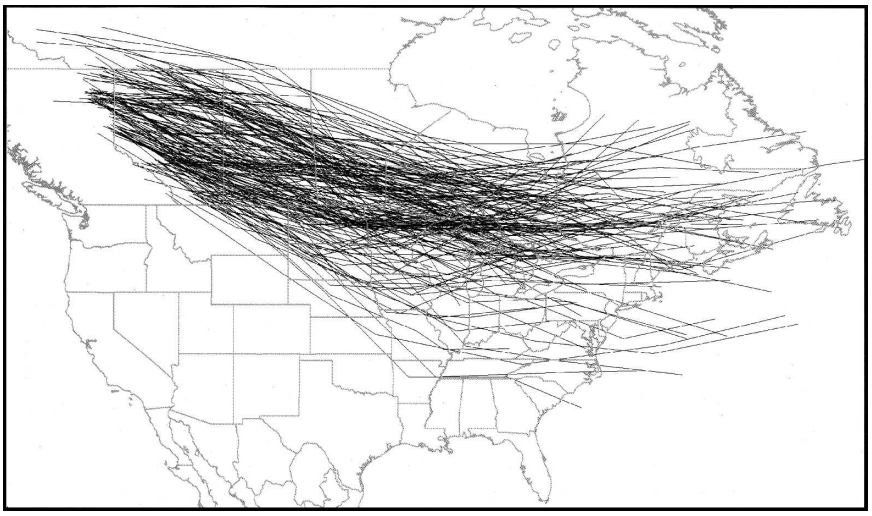

FIG. 1. Storm tracks of all Alberta clippers in the climatology out to 60 h after departure.

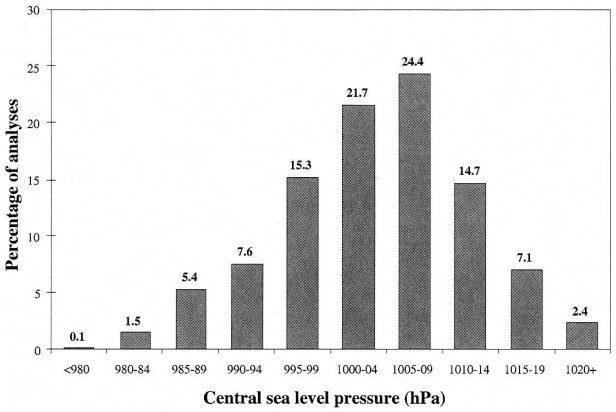

FIG. 2. Distribution of central SLP recorded at every 12-h analysis time during the 60-h postdeparture period for all clippers in the climatology. A total of 1062 SLP values were recorded.

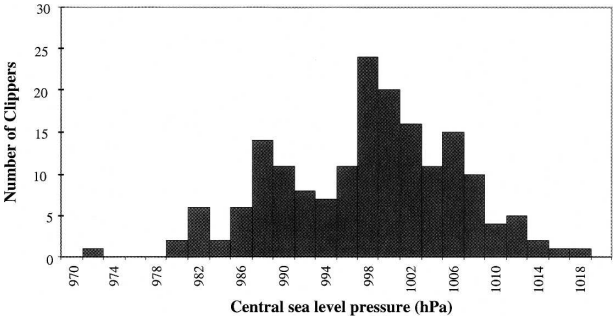

FIG. 3. Distribution of lowest central SLP (in 2-hPa bins) during the 60-h postdeparture period for all clippers in the climatology. The pressure value given is the upper limit of each respective bin.

geostrophic winds and thus should not be considered to have identical intensities. A reference latitude of 50°N is chosen because it is the mean latitude of clippers in the 60-h postdeparture period.

The distribution of central SLP values recorded at 12-h intervals from departure to 60 h after departure for all clippers in the climatology is given in Fig. 2. The clippers have a central SLP between 1000 and 1009 hPa during 46% of the total analysis times. A similar frequency of relatively high central SLP was found for winter cyclones moving east-southeast or south-southeast through the Midwest (Hurley 1954) and for winter cyclones over the Great Lakes (Harman et al. 1980; Angel and Isard 1998). Though the distribution is skewed toward lower pressure (largely an effect of the relatively high pressure at which the peak of the distribution is located), the central SLP of clippers is ≤990 hPa in only 7% of the analyses. The relatively weak nature of most clippers is further illustrated by the concentration toward higher values in the distribution of lowest central SLP attained for all clippers during the 60-h postdeparture period (Fig. 3). Only 28% of cases reach a central SLP ≤ 992 hPa, the benchmark used by Angel and Isard (1997) to define a "strong" cyclone.

Changes in clipper strength can be determined more explicitly by examining the distribution of adjusted 12-h SLP tendency (Fig. 4). Clippers experience minor SLP changes [$|dp/dt| \leq 2$ hPa (12 h)$^{-1}$] during ~37% of all 12-h periods. Periods of moderate [2–6 hPa (12 h)$^{-1}$] pressure rises outnumber periods of moderate pressure falls by about 10% (~29% versus ~19%), while the frequency of major [≥6 hPa (12 h)$^{-1}$] pressure rises and falls, though nearly equal, is quite small (~7%).

The distribution of maximum 12-h deepening rates for clippers during the postdeparture period is shown in Fig. 5. The distribution is qualitatively similar to the maximum deepening rate distribution for continental cyclones presented in Roebber (1989, Fig. 2c). About 53% of the clippers in the climatology have a maximum deepening rate of 2–6 hPa (12 h)$^{-1}$ (i.e., a moderate pressure fall). Only 10 of 177 clippers experience a maximum deepening rate ≥10 hPa (12 h)$^{-1}$, the approximate threshold rate for explosive cyclogenesis at 50°N (Sanders and Gyakum 1980). All but one of these explosive cyclogenesis periods occur either at 48 or 60 h after departure time as rapidly moving clippers near or move over the Atlantic coast, where dynamic and thermodynamic conditions are generally most favorable for rapid cyclone development. Interestingly, the number of clippers that experience filling throughout the 60-h postdeparture period (15) is higher than the number of clippers that undergo explosive cyclogenesis at any time during the postdeparture period (10).

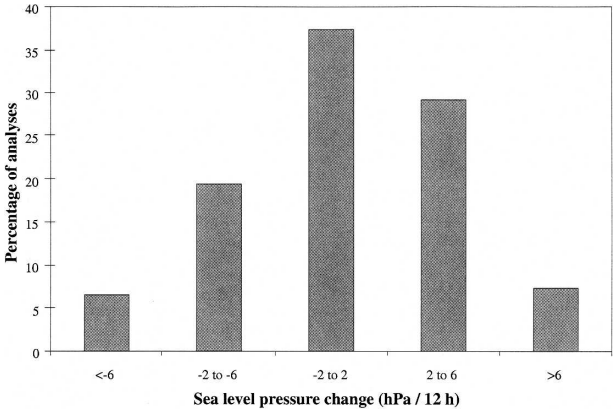

FIG. 4. Distribution of adjusted SLP tendency [hPa (12 h^{-1})] recorded in every 12-h interval during the 60-h postdeparture period for all clippers in the climatology.

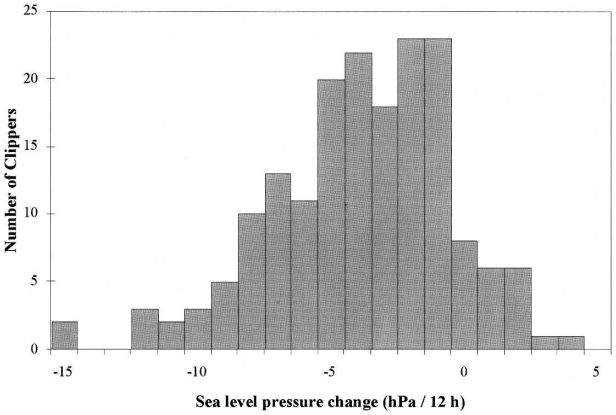

FIG. 5. Distribution of maximum clipper deepening rates [hPa $(12\ h)^{-1}$] during the 60-h postdeparture period.

4. Structure and evolution of the composite Alberta clipper

Although substantial intercase variability is found among the 177 cases selected for the Alberta clipper climatology, a significant number of common elements in the structure and evolution of these storms were also evident. These common features will be highlighted through an analysis of the composite structure and evolution of the clipper. The composite analysis will describe the evolution of the composite cyclone at 12-h intervals through two distinct stages: 1) a period of 36 h leading up to the time of departure (i.e., the *predeparture* period) and 2) a period of 60 h after departure (i.e., the *postdeparture* period).

a. Construction of the composites

A compositing procedure similar to that used by McLay and Martin (2002) was utilized in this study. The composite construction process first involved the definition of a composite grid. The composite grid at a given analysis time was chosen to have dimensions (in meters) equivalent to those of a 40° latitude × 180° longitude domain centered at the average position of the clipper's sea level pressure minimum at T = 0 h for each analysis time in the predeparture period and at the corresponding average position of the clipper's sea level pressure minimum for each of the 12-h intervals in the postdeparture period (Fig. 6). The numbers of grid points in the zonal and meridional directions (73 and 17 points, respectively) were fixed. The distance separating the grid points in the zonal direction is a function of grid row while the distance separating the grid points in the meridional direction is a constant, equivalent to the distance associated with a 2.5° increment in latitude. Having defined the composite grid, the following procedure was then used for the case-by-case construction of the composites. For a given cyclone and analysis time, the following steps were taken.

1) All basic-state variables (such as geopotential height) were placed on the ECMWF latitude–longitude grid.
2) The ECMWF grid point closest to the location of the cyclone's sea level pressure minimum was determined. For analysis times in the predeparture period, the closest grid point to the location of the

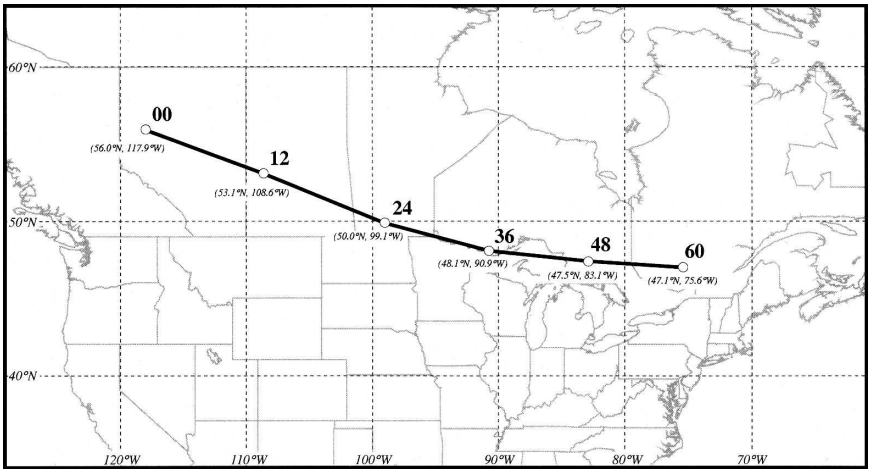

FIG. 6. Gray dots represent the average position of all Alberta clippers in the climatology at the given time (h) after departure. The black line connecting the dots represents the average track of the Alberta clippers in the climatology. Latitude and longitude of each average position are indicated.

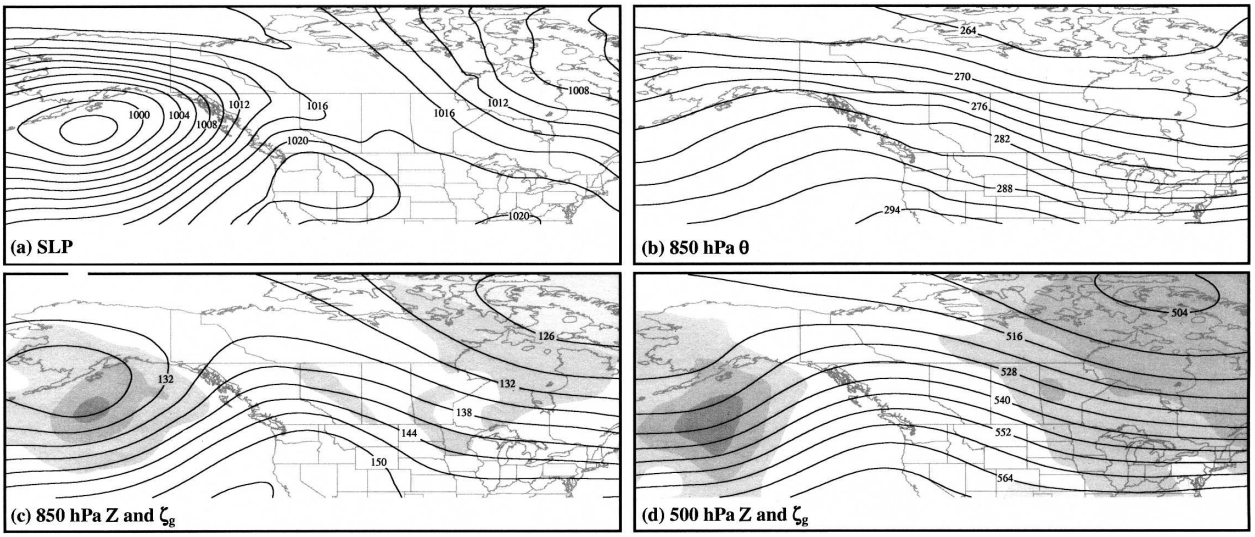

FIG. 7. Composite analyses for all Alberta clippers at $T - 36$ h. (a) Composite SLP (hPa) contoured every 2 hPa. (b) Composite 850-hPa potential temperature (K) contoured every 3 K. (c) Composite 850-hPa geopotential height (dam; solid lines) contoured every 3 dam and 850-hPa geostrophic relative vorticity (shading). Shading for geostrophic relative vorticity begins at 5×10^{-6} s^{-1} with a shading interval of 10×10^{-6} s^{-1}. (d) As in (c) but at 500 hPa and contoured every 6 dam.

cyclone's SLP minimum at $T = 0$ h for a given case was used.

3) The grid point determined in step 2 was taken to represent the center of the composite grid. The composite grid was then "overlain" on the ECMWF latitude–longitude grid such that a given row of the composite grid was superimposed with a given row on the ECMWF grid.
4) A particular grid point on the composite grid was selected. The closest ECMWF grid points to the west and east of this composite grid were located. The values of each variable at these ECMWF grid points were then linearly interpolated to obtain the value of each variable at the composite grid point. This step was repeated for all composite grid points.

After completing steps 1–4 for all clippers in the climatology at a particular analysis time, the composite distribution at that analysis time of a given variable was then constructed by taking the average of that variable at each of the grid points within the composite grid.

b. *Development of the composite clipper in the predeparture period*

The predeparture period for the composite clipper is marked by three major features: a cyclone over the Gulf of Alaska, a tropospheric deep ridge over western North America, and a lee trough developing east of the Canadian Rockies in British Columbia and Alberta. These features are reflected in the composite SLP field at $T - 36$ h (Fig. 7a) as a SLP minimum centered in the southwestern Gulf of Alaska, an anticyclone over the Intermountain West, and a weak trough of low pressure from northern British Columbia to southeastern Alberta. Associated with the Gulf of Alaska cyclone is a broad thermal ridge at 850 hPa over the northeastern Pacific Ocean (Fig. 7b). A more subtle thermal ridge is located in the lee of the Canadian Rockies, with a strong northwest–southeast-oriented baroclinic zone extending from northern Alberta to the western Great Lakes region (Fig. 7b). The Gulf of Alaska cyclone has prominent short-wave geostrophic relative vorticity maxima at 850 and 500 hPa (Figs. 7c and 7d) embedded within a larger-scale trough over the northern Pacific Ocean. Evidence for the lee trough in the vorticity[5] field is seen only at 850 hPa (Fig. 7c).

At $T - 12$ h, the center of the surface cyclone in the Gulf of Alaska is just south of the southern Alaska coast with little change in central SLP (Fig. 8a). The anticyclone over the Intermountain West has shifted slightly eastward and its central pressure has increased. The lee trough continues to broaden and become better defined. The axis of the 850-hPa thermal ridge connected with the Gulf of Alaska cyclone lies parallel to and just off the coastline with little change in its amplitude (Fig. 8b). Continuing cross-mountain flow has further increased the 850-hPa potential temperature over

[5] For brevity, geostrophic relative vorticity will be referred to as simply "vorticity" throughout this paper.

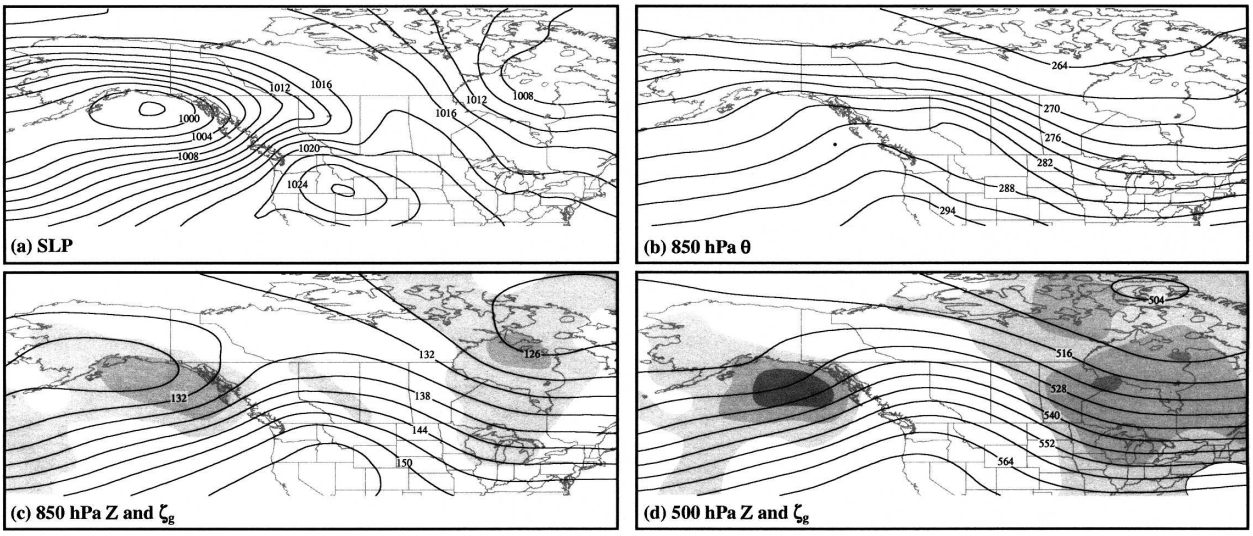

FIG. 8. As in Fig. 7 but for $T - 12$ h.

southern Alberta, enhancing the baroclinic zone over northeastern Alberta and Saskatchewan. As with the SLP minimum, the vorticity maxima at 850 and 500 hPa associated with the Gulf of Alaska cyclone are very close to the coast (Figs. 8c and 8d). The magnitude of the 850-hPa vorticity maximum has decreased slightly (Fig. 8c), a likely result of the interaction of the low-level flow with the coastal orography and the encroachment of the vorticity maximum upon the ridge to its east. The 500-hPa vorticity maximum experiences little change in its magnitude as it nears the coast (Fig. 8d). Only a slight indication of the lee trough is found in the 850-hPa geopotential height and vorticity fields (Fig. 8c), with no indication of the trough at 500 hPa (Fig. 8d).

Substantial changes occur in the last 12 h before departure, as evidenced by the composite fields from $T = 0$ h (Fig. 9). The SLP minimum in the Gulf of Alaska has weakened dramatically as the center of the surface cyclone interacts with the orography along the coast (Fig. 9a). The center of the surface anticyclone in the Intermountain West has shifted slightly southeastward and weakened considerably. Broadening of the lee trough has continued, and an elongated area of low pressure links the Gulf of Alaska cyclone and the lee trough. Within the lee trough, a closed low pressure center has developed. With the landfall of the Gulf of Alaska cyclone, the amplitude of the 850-hPa thermal ridge (Fig. 9b) and magnitude of the 850-hPa vorticity maximum (Fig. 9c) associated with the Gulf of Alaska cyclone have greatly decreased. Over the lee of the Canadian Rockies, the 850-hPa thermal ridge has become more prominent with the thermal ridge axis positioned over the composite SLP minimum (Fig. 9b). A relatively strong 850-hPa vorticity maximum has formed within the lee trough, with the center of the vorticity maximum just east of the SLP minimum (Fig. 9c). The 500-hPa vorticity maximum associated with the Gulf of Alaska cyclone has nearly scaled the ridge over western North America (Fig. 9d), undergoing a decrease in its magnitude in the process. The 500-hPa ridge axis over western North America has shifted to a position just east of the SLP minimum.

c. *Summary of the predeparture period*

The development of nearly every clipper in the climatology is preceded by the landfall of a cyclone along the coastline of Alaska or British Columbia. These cyclones typically progress northeastward and fill as they approach the coastal mountain ranges bordering the northeast Pacific Ocean. A strong northward component in movement and an increase in central SLP are characteristic of almost all surface cyclones as they near major mountain ranges (e.g., Palmén and Newton 1969; Chung et al. 1976), with frequent dissipation of cyclones in the northeast Pacific Ocean (Petterssen 1956; Zishka and Smith 1980; Roebber 1984; Bell and Bosart 1989; Lefevre and Nielsen-Gammon 1995). The composite results suggest the dissipation of a Pacific cyclone and the development of a new cyclone in the lee of the Canadian Rockies within the standing lee trough (Figs. 7–9a), contrary to the suggestions of Hess and Wagner (1948) and Bannon (1992). They showed an amoeba-like motion of the surface cyclone as it crossed the mountains, giving the impression that the original cyclone never dissipates but jumps across the mountains.

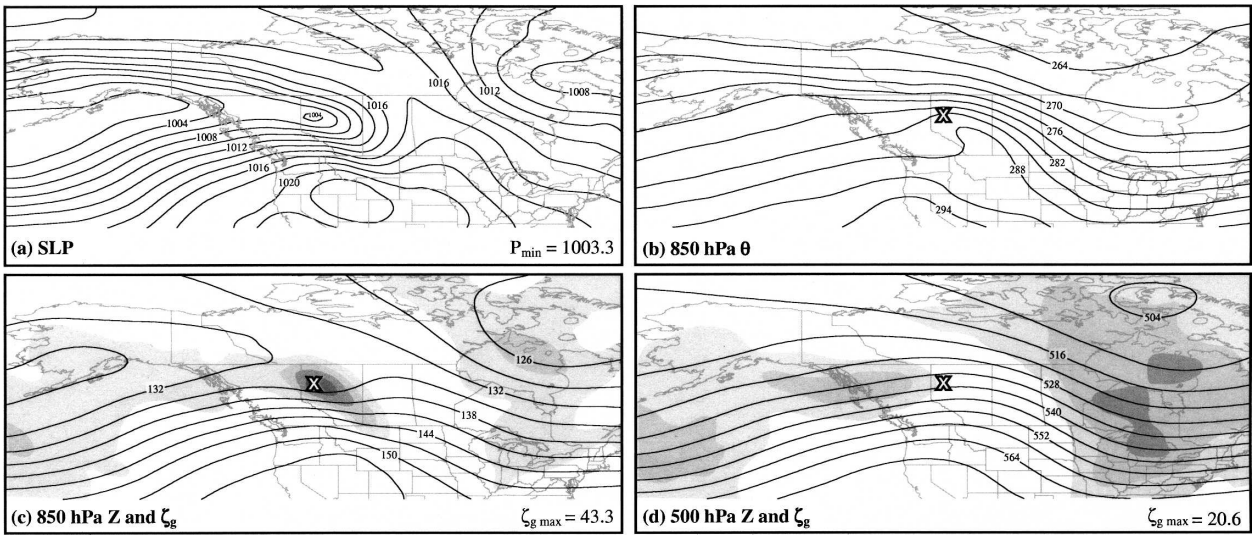

FIG. 9. As in Fig. 7 but for $T = 0$ h. Values in the lower-right corner of (a), (c), and (d) are the minimum SLP (hPa), maximum 850-hPa geostrophic relative vorticity ($\times 10^{-6}$ s^{-1}), and maximum 500-hPa geostrophic relative vorticity ($\times 10^{-6}$ s^{-1}), respectively. The X symbol in (b)–(d) corresponds to the location of the SLP minima of the composite clipper.

The 850-hPa baroclinic zone to the east of the Canadian Rockies remains nearly stationary through the predeparture period (Figs. 7–9b). As the Pacific cyclone nears the west coast of North America, cross-mountain flow strengthens and adiabatic warming from downslope flow in the lee of the Canadian Rockies increases. In the composite, the greatest adiabatic warming occurs to the south of the eventual position of the composite clipper SLP minimum at departure time. The presence of a lee trough from $T - 36$ h to $T - 12$ h is manifest as a region of small 850-hPa vorticity on the east side of the Canadian Rockies (Figs. 7c and 8c). By $T = 0$ h (Fig. 9c), a more pronounced short-wave trough and substantially stronger vorticity maximum are shown over the lee of the Canadian Rockies. Though the composite does not unambiguously reveal whether the 850-hPa vorticity maximum associated with the Pacific cyclone propagates over the mountains and the strong ridge or if a new vorticity maximum forms in the lee of the Canadian Rockies as a response to the development of the surface lee cyclone, the sudden increase in vorticity over the last 12 h of the predeparture is most likely the result of differential vertical motion (i.e., descent at low levels, ascent at upper levels) and attendant column stretching.

It is clear from the composite that the 500-hPa vorticity maximum scales the ridge over western North America (Figs. 7–9d) during the predeparture period. Though weakened by its passage over the ridge, the 500-hPa vorticity maximum is located well west of the SLP minimum at departure time. Encroachment of the upper-level trough axis on the lower-tropospheric thermal ridge axis was identified by Carlson (1961) as the central characteristic of the transition from stationarity to mobility for a lee trough.

d. Structure and evolution of the composite clipper in the postdeparture period

At $T + 12$ h (Fig. 10), the center of the composite clipper system has moved into far western Saskatchewan. The SLP minimum has deepened by about 1 hPa (Fig. 10a) with troughs of low pressure extending to the south-southeast and west-northwest of the surface cyclone center.[6] The 850-hPa thermal ridge remains strongly amplified (Fig. 10b), with the thermal ridge axis collocated with the SLP trough south of the composite clipper center. The thermal ridge is also collocated with the 850-hPa geopotential height trough (Fig. 10c), characteristic of a lee trough structure (e.g., Bluestein 1993, p. 13). The 850-hPa vorticity maximum has increased in magnitude while embedded in northwesterly flow and is centered directly over the SLP minimum (Fig. 10c). The magnitude of the 500-hPa vorticity maximum has also increased (Fig. 10d), but remains substantially less than that of the 850-hPa vorticity maximum. Importantly, the center of the 500-hPa vorticity maximum lies slightly to the west of the SLP minimum.

The central SLP of the composite clipper is slightly

[6] Such SLP troughs characterize the majority of individual clipper cases as determined by inspection of a large number of operational surface analyses (not shown).

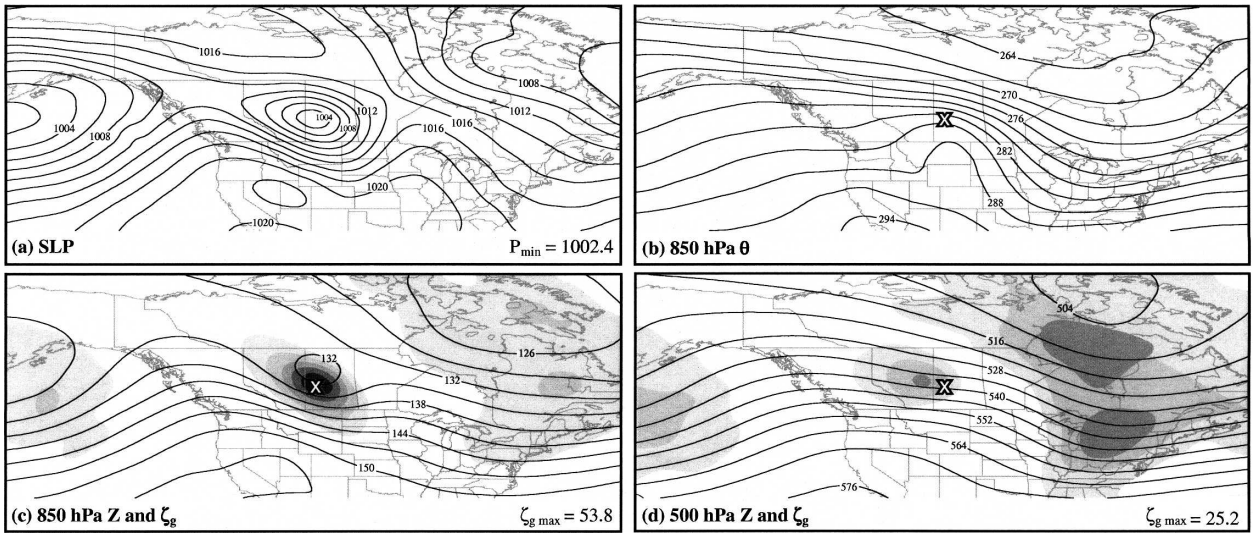

FIG. 10. As in Fig. 9 but for T + 12 h.

higher at T + 24 h (Fig. 11a), with troughs of low pressure extending to the south and west-northwest from the SLP minimum. A surface anticyclone has become evident to the northwest of the composite clipper. The amplitude of the thermal ridge at 850 hPa (Fig. 11b) has decreased slightly, and the thermal ridge axis has moved to just east of the SLP trough extending south from the composite clipper center while taking on a southwest–northeast orientation. Colder air is beginning to filter southward to the west-northwest of the SLP minimum as evidenced by the subtle depression in the 850-hPa isentropes. The thermal ridge axis remains nearly collocated with the 850-hPa geopotential trough (Fig. 11c). The 850-hPa vorticity maximum continues increasing in magnitude within a compact short-wave trough, with the center of the vorticity maximum remaining almost directly over the SLP minimum. The strengthening 500-hPa vorticity maximum (Fig. 11d) continues to have a smaller magnitude than its counterpart at 850 hPa and remains west of the SLP minimum.

Filling of the composite SLP minimum continues through T + 36 h (Fig. 12a). The once well-defined troughs of low pressure emanating from the SLP minimum appear to have merged into one broad trough to the southwest of the surface cyclone center. The anticyclone to the northwest of the composite clipper has shifted southeastward with little change in its intensity.

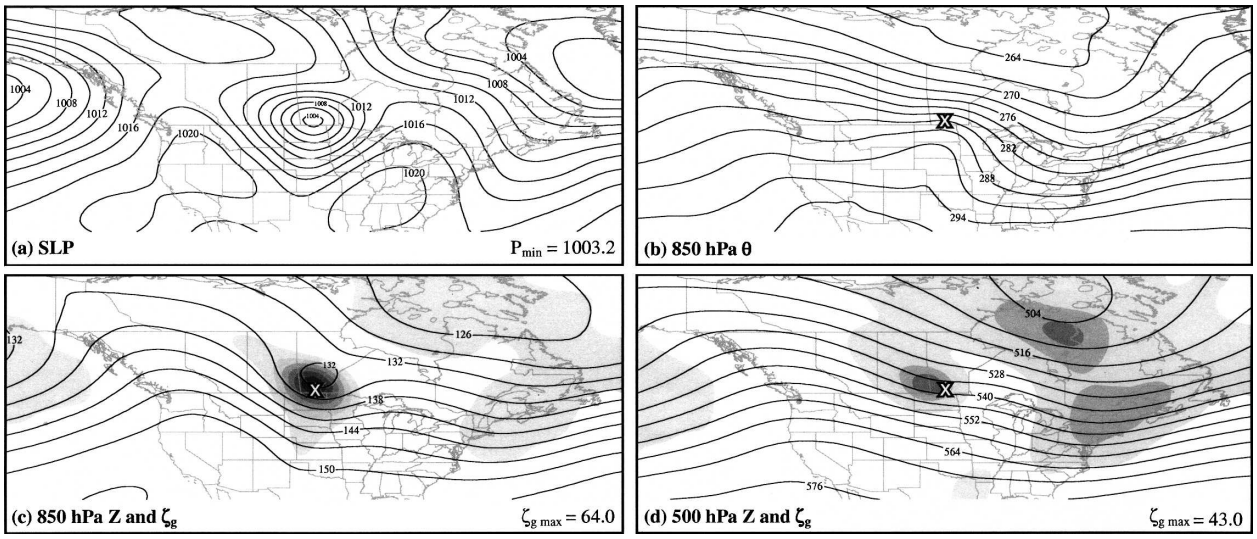

FIG. 11. As in Fig. 9 but for T + 24 h.

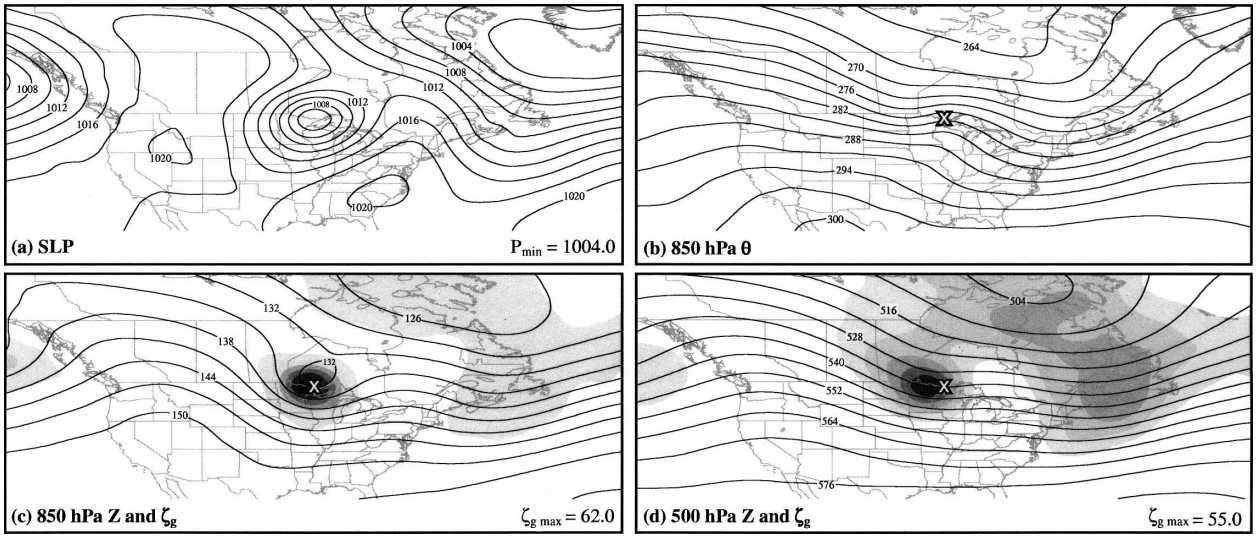

FIG. 12. As in Fig. 9 but for T + 36 h.

The 850-hPa thermal ridge is substantially less amplified (Fig. 12b), and colder air to the west of the SLP minimum has continued to surge southward. The 850-hPa thermal ridge axis has rotated slightly counterclockwise and is positioned just east of the SLP minimum. The 850-hPa vorticity maximum has changed little in magnitude, but the center has moved slightly to the west of the SLP minimum (Fig. 12c). The 500-hPa vorticity maximum has increased to a magnitude only slightly less than that of the 850-hPa vorticity maximum and remains centered to the west of the SLP minimum (Fig. 12d).

The SLP minimum continues its steady filling at T + 48 h with little evidence of distinct troughs extending from the center of the cyclone (Fig. 13a). A broad region of high pressure is in place west of the SLP minimum with the melding of the anticyclones from Canada and the northern U.S. Rocky Mountains. The 850-hPa thermal ridge maintains its smaller amplitude, but the thermal ridge axis has further rotated counterclockwise into a north–south orientation (Fig. 13b). The 850-hPa vorticity maximum has decreased in magnitude and continues to be centered slightly west of the SLP minimum (Fig. 13c). The 500-hPa vorticity maximum has increased to a magnitude exceeding that of the 850-hPa vorticity maximum and remains centered well west of the SLP minimum (Fig. 13d).

The steady filling of the composite SLP minimum

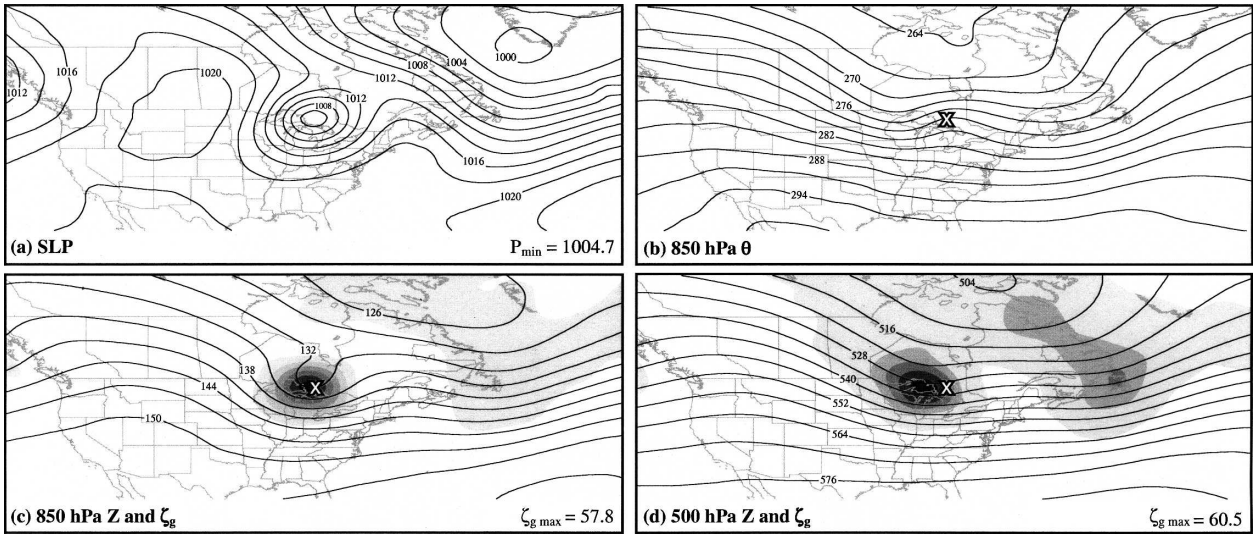

FIG. 13. As in Fig. 9 but for T + 48 h.

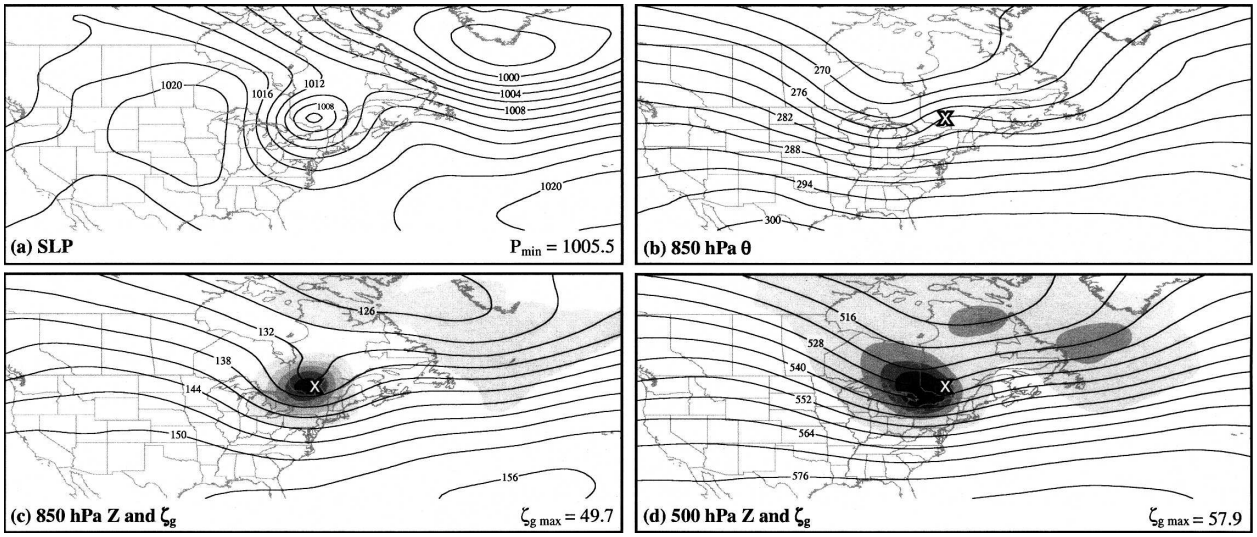

FIG. 14. As in Fig. 9 but for T + 60 h.

continues through T + 60 h (Fig. 14a). A broad anticyclone is now positioned over central North America. The 850-hPa thermal ridge axis has rotated into a northwest–southeast orientation with little change in its amplitude, and cold air continues pushing southward to the west of the composite clipper center (Fig. 14b). The 850-hPa vorticity maximum continues to weaken (Fig. 14c), while the 500-hPa vorticity maximum maintains its strength (Fig. 14d). A structure conducive for baroclinic development is exhibited by the composite clipper as clear westward displacement of the vorticity centers with height is evident (Figs. 14c and 14d).

e. Summary of the postdeparture period

The composite Alberta clipper is not a particularly robust cyclone in terms of its central SLP or its size. In fact, the composite clipper reaches its lowest central SLP (1002.4 hPa) at T + 12 h, with a steady pressure increase of 0.7–0.8 hPa every 12 h through T + 60 h (Figs. 10–14a). Though the central SLP of the composite clipper is relatively high, the system is flanked by anticyclones to its south and northwest that lead to relatively strong pressure gradients around the composite clipper center.

The composite 850-hPa potential temperature field (Figs. 10–14b) undergoes substantial change during the postdeparture period. Adiabatic warming from downslope flow creates an amplified thermal ridge in the first 24 h after departure. This enhanced thermal ridge maintains a strong baroclinic zone north and northeast of the composite clipper center. The thermal ridge axis is collocated with the SLP trough early in the postdeparture period, with the peak of the thermal ridge near the composite SLP minimum. This structure clearly resembles a lee trough structure (e.g., Bluestein 1993, p. 13).

Substantial dampening of the thermal ridge occurs between T + 24 h and T + 36 h (Figs. 11–12b), a direct consequence of the cessation of adiabatic warming from downslope flow to the west of the composite clipper center as the system moves farther away from the Rockies. The thermal ridge axis also shifts to a position slightly to the east of the SLP minimum and associated southward-extending SLP trough. Previously blocked by the higher terrain, colder air to the northwest of the composite clipper center funnels southward as the system progresses away from the Rockies. The southward progression of the baroclinic zone to the west of the composite SLP minimum and the apparent merging of the two distinct pressure troughs at T + 24 (Fig. 11a) into one broad trough at T + 36 (Fig. 12a) mark the process of the cold front overtaking the lee trough. Over the last 24 h of the postdeparture period, the baroclinic zones take on an orientation resembling that of the cold and warm fronts in a classical cyclone (Bjerknes and Solberg 1922). Locatelli et al. (1989) and Steenburgh and Mass (1994) describe a similar transition in structure from a lee trough to a more classical midlatitude cyclone over approximately the same time frame as shown in this study.

Though the central SLP of the composite cyclone is relatively high, the cyclonic circulations associated with the composite system are well defined at both 850 and 500 hPa as evidenced by the magnitude of the geostrophic relative vorticity (Figs. 10–14c,d). The magnitude of the 850- (500-) hPa vorticity maximum is largest

during the early (late) stages of the postdeparture period (Figs. 10–14c,d), suggesting that the lower-tropospheric circulation of the clipper is strongest early in the life cycle, while the upper-tropospheric circulation strengthens throughout the life cycle. The positioning of the vorticity maxima with respect to the SLP minimum also sheds light on the nature of the evolving clipper system. The maximum 850-hPa vorticity is located directly above the SLP minimum through the first 24 h of the postdeparture period, shifting slightly to the west of the SLP minimum over the last 36 h of the postdeparture period. At 500 hPa, the center of the vorticity maximum remains well west of the SLP minimum throughout the postdeparture period, a configuration favorable for cyclone development and propagation. Thus, analysis of the evolving thermal and geopotential height fields suggests that the composite clipper acquires a structure more favorable for baroclinic growth (e.g., Holton 1992) as time progresses.

5. Composite QG forcing for ascent

Additional insight into the nature of the Alberta clipper can be gleaned by considering the QG forcing for ascent throughout the clipper life cycle. The characteristic precipitation pattern of the clipper is directly related to the distribution of vertical motion, which is driven by both synoptic-scale and frontogenetical processes. Many studies have stressed the importance of the upper-level vorticity maximum and associated vorticity advection on the development and evolution of cyclones originating from the Canadian Rockies (e.g., Hess and Wagner 1948; McClain 1960; Palmén and Newton 1969; Steenburgh and Mass 1994). Frontal-scale processes also can contribute greatly to forcing for vertical motion in cyclones that are generated in the lee of the Canadian Rockies (Locatelli et al. 1989; Martin et al. 1990; Steenburgh and Mass 1994; Kapela et al. 1995). The forcing produced by synoptic-scale and frontogenetical processes can be separately diagnosed from a QG perspective by considering the **Q**-vector form of the QG omega equation:

$$\left(\sigma\nabla^2 + f_o\frac{\partial^2}{\partial p^2}\right)\omega = -2\nabla\cdot\mathbf{Q} \tag{1}$$

(Hoskins et al. 1978). For adiabatic, geostrophic flow, **Q** represents the rate of change of the potential temperature gradient vector ($\nabla\theta$) on an f plane along a geostrophic trajectory:

$$\mathbf{Q} = f\gamma\frac{d}{dt_g}\nabla_p\theta, \tag{2}$$

where $\gamma = R/fp_o(p_o/p)^{c_v/c_p}$, $d/dt_g = \partial/\partial t + u_g\partial/\partial x + v_g\partial/\partial y$, the subscript g denotes geostrophic, and the subscript p denotes differentiation on an isobaric surface. Keyser et al. (1992) showed that a partition of **Q** into across- and along-isentrope components describes changes in the magnitude and direction of $\nabla\theta$, respectively. Employing the natural coordinate system adopted by Martin (1999), the across-isentrope component of **Q** is given by

$$\mathbf{Q}_n = \frac{\mathbf{Q}\cdot\nabla\theta}{|\nabla\theta|}\left(\frac{\nabla\theta}{|\nabla\theta|}\right) = Q_n\mathbf{n} \tag{3}$$

and is physically related to changes in the magnitude of $\nabla\theta$. Note that the scalar function Q_n is identically equal to the QG frontogenesis function ($F_g = d/dt_g|\nabla\theta|$); thus, $-2\nabla\cdot\mathbf{Q}_n$ represents the forcing for vertical motion associated with frontogenetical processes. The along-isentrope component of **Q** is given by

$$\mathbf{Q}_s = \frac{\mathbf{Q}\cdot(\mathbf{k}\times\nabla\theta)}{|\nabla\theta|}\left(\frac{\mathbf{k}\times\nabla\theta}{|\nabla\theta|}\right) = Q_s\mathbf{s} \tag{4}$$

and is related to the rate of change of direction of $\nabla\theta$. Keyser et al. (1992) referred to $-2\nabla\cdot\mathbf{Q}_s$ as the "wave scale" forcing for ω. Support for this assertion arises from a recent study of cyclones from the QG ω perspective that identifies $-2\nabla\cdot\mathbf{Q}_s$ as the predominant forcing associated with synoptic-scale development (Martin 2006). Given their relationships to $\nabla\theta$, examination of each component of **Q** provides insight into the dynamical processes that underlie the changes in the thermal structure of the composite clipper during the postdeparture period.[7]

Figure 15 shows the 850-hPa composite potential temperature and $\mathbf{Q}_n$ vectors of the composite[8] at $T + 12$ h, $T + 36$ h, and $T + 60$ h. Recalling that $\mathbf{Q}_n = F_g\mathbf{n}$, the evolution of the geostrophic frontogenesis throughout the clipper life cycle is reflected in the distribution and direction of $\mathbf{Q}_n$. At $T + 12$ h (Fig. 15a), the strongest geostrophic frontogenesis is located well east of the composite SLP minimum along the broad northwest–southeast-oriented baroclinic zone, while geostrophic frontolysis is occurring to the northwest of the SLP minimum. Geostrophic frontogenesis continues to the

[7] Selected cases were examined to compare the QG forcing calculated using available 1° × 1° data to that calculated using the 2.5° × 2.5° data. It was determined that the 2.5° data accurately depict the characteristics of the **Q**-vector convergence–divergence patterns.

[8] The components of the **Q** vector, $\mathbf{Q}_n$ and $\mathbf{Q}_s$, are calculated using the composite geostrophic wind and potential temperature. Thus, $\mathbf{Q}_n$ and $\mathbf{Q}_s$ vectors shown are not *composite* $\mathbf{Q}_n$ and $\mathbf{Q}_s$ vectors, but rather $\mathbf{Q}_n$ and $\mathbf{Q}_s$ vectors *of the composite*.

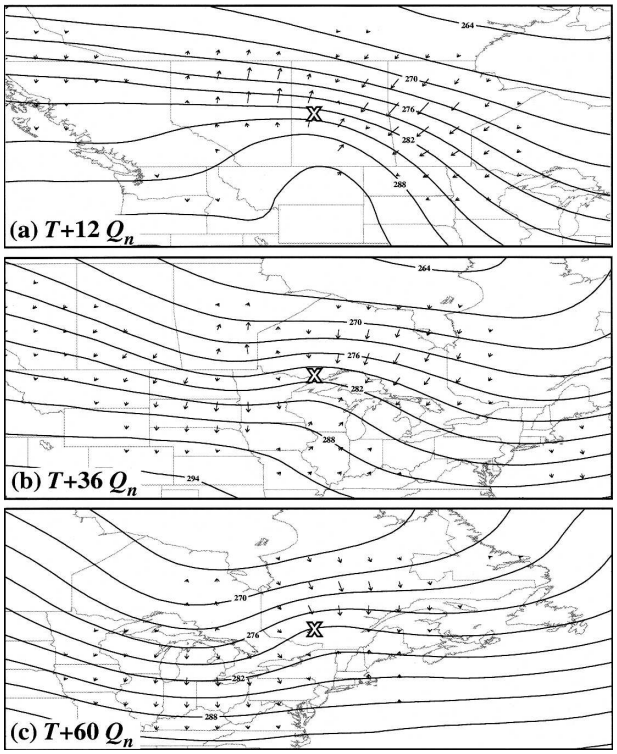

FIG. 15. Composite 850-hPa potential temperature (K) contoured every 3 K and 850-hPa $\mathbf{Q}_n$ vectors of the composite at (a) $T + 12$ h, (b) $T + 36$ h, and (c) $T + 60$ h. The X symbols are as in Fig. 9.

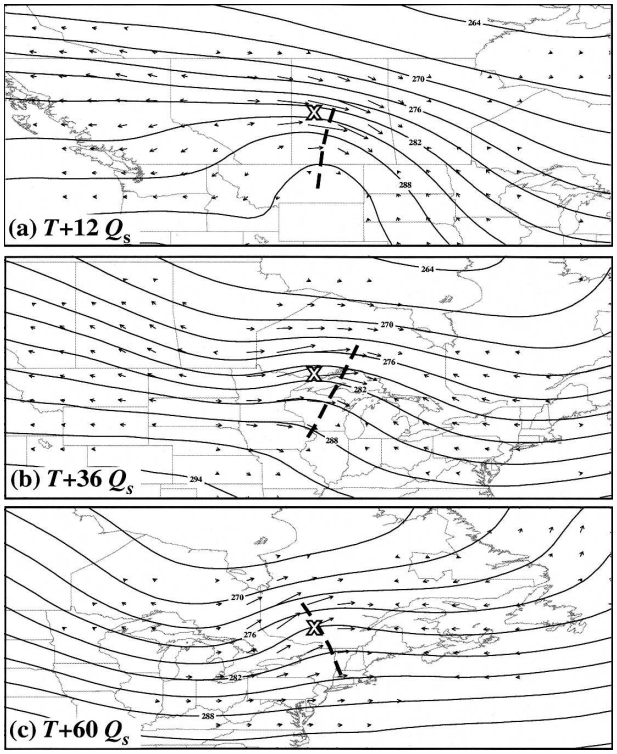

FIG. 16. As in Fig. 15 but for 850-hPa $\mathbf{Q}_s$ vectors of the composite. The thick dashed line represents the 850-hPa thermal ridge axis.

east and northeast of the composite SLP minimum at $T + 36$ h (Fig. 15b), though its magnitude is slightly less than it was 24 h earlier. Geostrophic frontogenesis is also occurring west of the composite SLP minimum along the southward-propagating cold front that was previously blocked by the orography. The thermal structure has taken on a more classical appearance with a warm-frontal baroclinic zone extending east and a cold-frontal baroclinic zone running west-southwest from the center of the cyclone. The more classical structure of the thermal field is maintained at $T + 60$ h (Fig. 15c) with distinct areas of geostrophic frontogenesis along the apparent warm and cold fronts. The strongest geostrophic frontogenesis remains along the warm front, though the magnitude of the frontogenesis along both fronts is slightly less than it was at $T + 36$ h.

The 850-hPa composite potential temperature and $\mathbf{Q}_s$ vectors of the composite are shown in Fig. 16. Throughout the postdeparture period, $\mathbf{Q}_s$ vectors with the greatest magnitude are located near the thermal ridge axis. As a result, the greatest rotation of the thermal gradient vector will occur in the baroclinic zone near the thermal ridge axis. From $T + 12$ h to $T + 36$ h (Figs. 16a and 16b), the baroclinic zone along the top portion of the thermal ridge rotates counterclockwise from a northwest–southeast orientation to a largely west–east orientation. As the composite clipper moves into eastern North America between $T + 36$ h and $T + 60$ h (Figs. 16b and 16c), the baroclinic zone and the thermal ridge axis undergo a considerable counterclockwise rotation. Slight amplification of the thermal trough to the west of the composite SLP minimum is also apparent between $T + 36$ h and $T + 60$ h, a result of $\mathbf{Q}_s$ divergence centered within the thermal trough. The rotation of the thermal gradient described by $\mathbf{Q}_s$ leads to the development of a more classical thermal structure in the composite clipper.

The $\mathbf{Q}_n$ and $\mathbf{Q}_s$ components of $\mathbf{Q}$ and their respective divergences computed from the 500–850-hPa layer-averaged composite geostrophic wind and potential temperature at $T + 12$ h , $T + 36$ h, and $T + 60$ h are shown in Fig. 17. At $T + 12$ h, the convergences of $\mathbf{Q}_n$ and $\mathbf{Q}_s$ are comparable in magnitude and located well east of the SLP minimum (Figs. 17a and 17b). The distribution of $\nabla \cdot \mathbf{Q}_n$ (Fig. 17a) clearly depicts a circulation along the warm-frontal baroclinic zone to the east of the composite SLP minimum. The east–west couplet of $\nabla \cdot \mathbf{Q}_s$ along the mean flow greatly resembles regions of cyclonic and anticyclonic vorticity advection about a

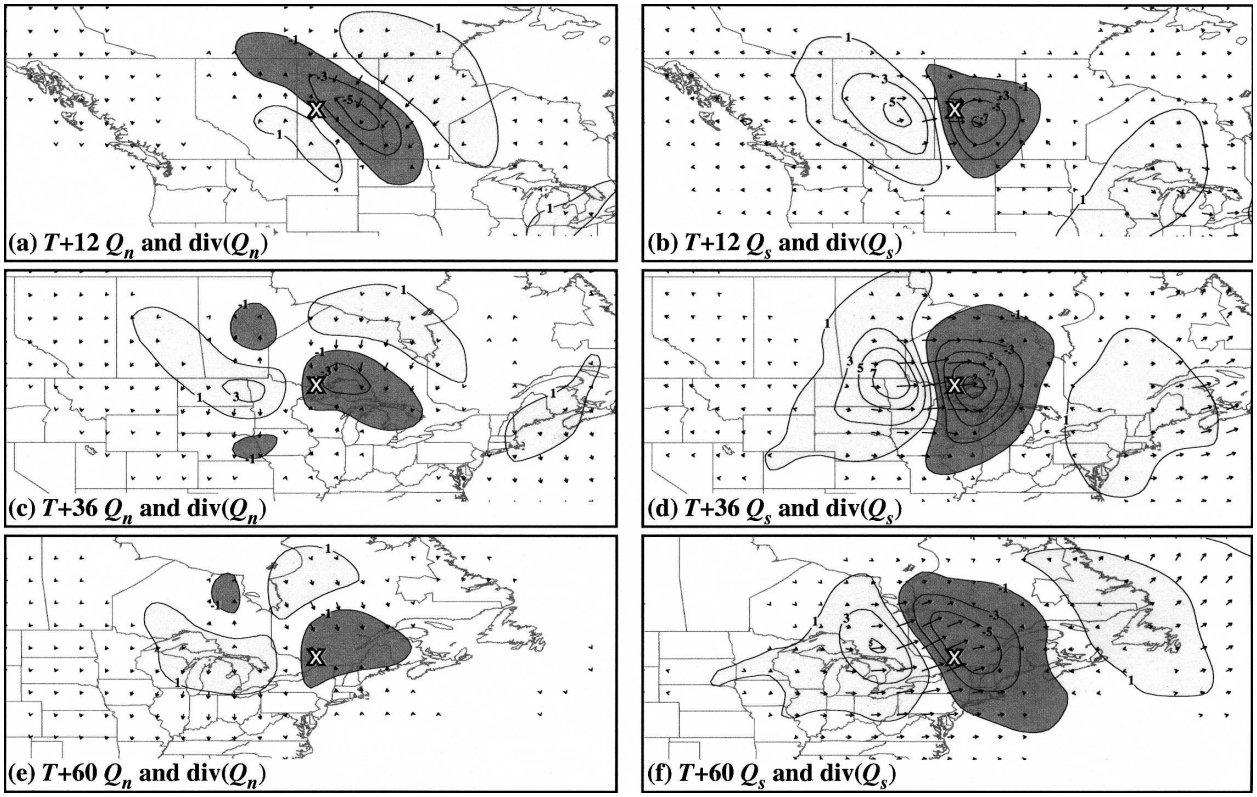

FIG. 17. (a) The 500–850-hPa layer-averaged $\mathbf{Q}_n$ vectors and $\mathbf{Q}_n$ divergence of the composite at $T + 12$ h. The $\mathbf{Q}_n$ divergence (convergence) is labeled in units of 10^{-16} m^2 s^{-1} kg^{-1}, indicated by light (dark) shading, and contoured every 2×10^{-16} m^2 s^{-1} kg^{-1}starting at 1 $(-1) \times 10^{-16}$ m^2 s^{-1} kg^{-1}. (b) As in (a) but for $\mathbf{Q}_s$ vectors and $\mathbf{Q}_s$ divergence at $T + 12$ h. (c) As in (a) but for $T + 36$ h. (d) As in (b) but for $T + 36$ h. (e) As in (a) but for $T + 60$ h. (f) As in (b) but for $T + 60$ h. The X symbols are as in Fig. 9.

vorticity maximum (Fig. 17b). By $T + 36$ h, the clipper has acquired more classical frontal features as evidenced by the warm-frontal circulation to the east and cold-frontal circulation to the west of the center of the composite clipper depicted in the $\nabla \cdot \mathbf{Q}_n$ field (Fig. 17c). The magnitude of $\nabla \cdot \mathbf{Q}_s$ has increased considerably (Fig. 17d), a reflection of the increased strength of the upper-level vorticity maximum in the composite. The collocation of relatively strong $\mathbf{Q}_n$ and $\mathbf{Q}_s$ divergence to the west of the composite SLP suggests that fairly strong subsidence occurs in that region. This subsidence, and its attendant downward transfer of momentum, likely contribute to the strong winds often experienced over central North America following the passage of cold fronts associated with clippers (Kapela et al. 1995). The magnitudes of $\nabla \cdot \mathbf{Q}_n$ and $\nabla \cdot \mathbf{Q}_s$ have decreased over all areas by $T + 60$ h (Figs. 17e and 17f), an indication of the slight weakening of the composite clipper. The frontal circulations about the composite SLP minimum (Fig. 17e) remain evident, though slightly weaker than 24 h earlier. Wave-scale processes continue to be the dominant contributor to QG forcing for vertical motion as the divergence and convergence of $\mathbf{Q}_s$ (Fig. 17f) remain considerably larger than the $\mathbf{Q}_n$ counterparts.

The composites provide compelling evidence of the evolution of the Alberta clipper from a lee trough to a more classically structured midlatitude cyclone. Orographic processes play an essential role in the building and maintenance of a prominent low-level thermal ridge early in the postdeparture period. As the clipper moves away from the immediate lee of the Rockies, the effects of orography are quickly lost and the thermal ridge undergoes rapid dampening. At the same time, synoptic-scale forcing becomes more dominant with the incorporation of the upper-level vorticity maximum into the clipper structure. The positioning of the 500-hPa vorticity maximum upstream of the SLP minimum allows for cyclonic vorticity advection by the thermal wind, a considerable portion of $-2\nabla \cdot \mathbf{Q}_s$ (Martin 1999), to occur over the surface cyclone. Here, $\mathbf{Q}_s$ is responsible for the geostrophic rotation of the thermal ridge that results in the development of a more classical thermal structure in the composite clipper. Thus, the ther-

mal gradient rotation necessary for the composite clipper to acquire a more classical thermal structure is dependent upon the upstream displacement of the 500-hPa vorticity maximum with respect to the surface cyclone center, which, in turn, fosters middle-tropospheric ascent associated with the clipper.

6. Conclusions

The Alberta clipper is one of the most prominent cold-season weather phenomena affecting central and eastern North America. Though often considered innocuous as a result of its rather weak signature in the SLP field and its associated meager precipitation amounts, the clipper can bring hazardous weather in the form of strong winds, blowing and drifting snow, and bitterly cold temperatures. Even with their frequent occurrence and acknowledged potential for producing dangerous weather, only a few studies have examined the clipper in detail. The present paper partially fills this surprising void by investigating the clipper via synoptic-climatological and composite analyses.

Many common characteristics were evident in the 177 Alberta clippers selected for the climatology. These common features were addressed through an analysis of the structure and evolution of the composite clipper. The first part of the analysis investigated the development of the composite clipper in the 36 h leading up to its departure from the lee of the Canadian Rockies. This predeparture period is marked by the following characteristics:

1) the approach and landfall of a Pacific cyclone whose mean SLP minimum and 850-hPa geopotential height minimum weaken considerably along the coastal mountain ranges of Alaska and British Columbia;
2) the development and eastward expansion of a standing lee trough in response to increasing cross-mountain flow and associated adiabatic warming with the approach of the Pacific cyclone toward the coast;
3) the development and amplification of a thermal ridge at 850 hPa in the lee of the Rockies primarily south of the departure point of the composite clipper resulting from increased adiabatic warming from persistent downslope flow;
4) the scaling of the ridge centered over the west coast of North America by the 500-hPa short-wave trough and associated vorticity maximum connected to the landfalling Pacific cyclone, which leads to their incorporation as part of the composite clipper structure at the time of departure; and
5) the development of a closed surface circulation in the lee trough at the time of departure.

The evolution of the variables above resembles findings shown in previous studies of lee cyclogenesis in the Canadian Rockies (e.g., Palmén and Newton 1969; Chung et al. 1976).

The second part of the analysis examined the structure and evolution of the composite clipper in the 60-h period following departure. Key features of note during the postdeparture period include the following.

1) The central SLP of the composite clipper remains relatively high throughout the postdeparture period, with the lowest SLP reached 12 h after departure followed by a steady rise in central SLP through the end of the postdeparture period.
2) The once-prominent 850-hPa thermal ridge formed primarily by adiabatic warming from downslope flow early in the postdeparture period dampens considerably as the composite clipper moves into central North America away from the immediate lee of the Canadian Rockies.
3) Cold air to the west of the composite clipper SLP minimum begins to filter southward starting 24 h after departure, as a cold front, previously blocked by higher terrain, rotates counterclockwise around the clipper. The cold front appears to overtake the lee trough ~36 h after departure.
4) The geostrophic relative vorticity maximum at 850 (500) hPa reaches its maximum magnitude early (late) in the postdeparture period, which suggests that the lower- (upper-) level circulation in the composite clipper is strongest early (late) in the life cycle.
5) Convergence of the along-isentrope component of the **Q** vector is the dominant contributor to QG forcing for vertical motion in the composite clipper throughout the postdeparture period, while QG forcing from frontogenetical processes is relatively weak and decreases over time.
6) An initially vertically stacked system at low levels acquires more westward tilt with height as the postdeparture period progresses. The 500-hPa short-wave trough and associated vorticity maximum always remain to the west of the composite SLP minimum throughout the postdeparture period.

As a whole, the composite clipper evolves from a lee trough to a more classical midlatitude cyclone as it moves through central and eastern North America. This evolution is largely accomplished through the counterclockwise rotation of the 850-hPa thermal ridge axis and the increasing westward tilt with the height of the composite clipper over the last 36 h of the postde-

parture period. The thermal gradient rotation is dynamically linked to cyclonic vorticity advection by the thermal wind and convergence of the along-isentrope (i.e., $\mathbf{Q}_s$) component of the **Q** vector made possible by the persistent westward displacement of the 500-hPa vorticity maximum with respect to the composite clipper SLP minimum. The nature and timing of the composite clipper evolution resembles the conceptual model of lee trough evolution described in Steenburgh and Mass (1994).

Acknowledgments. This paper represents a portion of the first author's M.S. thesis at the University of Wisconsin—Madison and was partially supported by a graduate fellowship provided by the American Meteorological Society and Lockheed Martin Missiles and Space. The authors thank Mr. Jason Otkin and Dr. Justin McLay for their assistance with the data conversion and compositing software and Mr. Pete Pokrandt for his general computer assistance. Constructive comments on the text from Profs. Michael Morgan and Eric DeWeaver are greatly appreciated. The insightful comments from three anonymous reviewers greatly enhanced the presentation in the manuscript.

REFERENCES

Angel, J. R., and S. A. Isard, 1997: An observational study of the influence of the Great Lakes on the speed and intensity of passing cyclones. *Mon. Wea. Rev.,* **125,** 2228–2237.

——, and ——, 1998: The frequency and intensity of Great Lakes cyclones. *J. Climate,* **11,** 61–71.

Bannon, P. R., 1992: A model of Rocky Mountain lee cyclogenesis. *J. Atmos. Sci.,* **49,** 1510–1522.

Beckman, S. K., 1987: Use of enhanced IR/visible satellite imagery to determine heavy snow areas. *Mon. Wea. Rev.,* **115,** 2060–2087.

Bell, G. D., and L. F. Bosart, 1989: A 15-year climatology of Northern Hemisphere 500 mb closed cyclone and anticyclone centers. *Mon. Wea. Rev.,* **117,** 2142–2163.

Bjerknes, J., and H. Solberg, 1922: Life cycle of cyclones and the polar front theory of atmospheric circulation. *Geofys. Publ.,* **12,** 1–61.

Bluestein, H. B., 1993: *Observations and Theory of Weather Systems.* Vol. II, *Synoptic–Dynamic Meteorology in Midlatitudes,* Oxford University Press, 594 pp.

Bonner, W. D., 1961: Development processes associated with the formation and movement of an Alberta cyclone. Tech. Rep. 4, Dept. of Meteorology, University of Chicago, 40 pp. [Available from Dept. of Geophysical Sciences, University of Chicago, 5743 S. Ellis Ave., Chicago, IL 60637.]

Carlson, T. N., 1961: Lee-side frontogenesis in the Rocky Mountains. *Mon. Wea. Rev.,* **89,** 163–172.

Chung, Y.-S., K. D. Hage, and E. R. Reinelt, 1976: On lee cyclogenesis and airflow in the Canadian Rocky Mountains and the east Asian mountains. *Mon. Wea. Rev.,* **104,** 879–891.

Davis, C. A., 1997: The modification of baroclinic waves by the Rocky Mountains. *J. Atmos. Sci.,* **54,** 848–868.

desJardins, M. L., K. F. Brill, and S. S. Schotz, 1991: Use of GEMPAK on UNIX workstations. Preprints, *Seventh Int. Conf. on Interactive Information and Processing Systems for Meteorology, Oceanography, and Hydrology,* New Orleans, LA, Amer. Meteor. Soc., 449–453.

Gallus, W. A., Jr., and J. F. Bresch, 1997: An intense small-scale wintertime vortex in the midwest United States. *Mon. Wea. Rev.,* **125,** 2787–2807.

Glickman, T. S., Ed., 2000: *Glossary of Meteorology.* 2d ed. Amer. Meteor. Soc., 790 pp.

Harman, J. R., R. Rosen, and W. Corcoran, 1980: Winter cyclones and circulation patterns in the western Great Lakes. *Phys. Geogr.,* **1,** 28–41.

Harms, R. W., 1973: Snow forecasting for southwestern Wisconsin. *Weatherwise,* **26** (12), 250–255.

Henry, A. J., 1925: Pressure over the northeastern Pacific, and weather in the United States, December, 1924, and January, 1925. *Mon. Wea. Rev.,* **53,** 5–10.

Hess, S. L., and H. Wagner, 1948: Atmospheric waves in the northwestern United States. *J. Meteor.,* **5,** 1–19.

Holton, J. R., 1992: *An Introduction to Dynamic Meteorology.* Academic Press, 509 pp.

Hoskins, B. J., and K. I. Hodges, 2002: New perspectives on the Northern Hemisphere winter storm tracks. *J. Atmos. Sci.,* **59,** 1041–1061.

——, I. Draghici, and H. C. Davies, 1978: A new look at the ω-equation. *Quart. J. Roy. Meteor. Soc.,* **104,** 31–38.

Hurley, J. C., 1954: Statistics on the movement of and deepening of cyclones in the Middle West. *Mon. Wea. Rev.,* **82,** 116–122.

Hutchinson, T. A., 1995: An analysis of NMC's Nested Grid Model forecasts of Alberta clippers. *Wea. Forecasting,* **10,** 632–641.

Kapela, A. F., P. L. Leftwich, and R. Van Ess, 1995: Forecasting the impacts of strong wintertime post-cold front winds in the northern plains. *Wea. Forecasting,* **10,** 229–244.

Keyser, D., B. D. Schmidt, and D. G. Duffy, 1992: Quasigeostrophic vertical motions diagnosed from along- and cross-isentrope components of the Q vector. *Mon. Wea. Rev.,* **120,** 731–741.

Lefevre, R. J., and J. W. Nielsen-Gammon, 1995: An objective climatology of mobile troughs in the Northern Hemisphere. *Tellus,* **47A,** 638–655.

Locatelli, J. D., J. M. Sienkiewicz, and P. V. Hobbs, 1989: Organization and structure of clouds and precipitation on the mid-Atlantic coast of the United States. Part I: Synoptic evolution of a frontal system from the Rockies to the Atlantic Coast. *J. Atmos. Sci.,* **46,** 1327–1348.

Martin, J. E., 1999: Quasigeostrophic forcing of ascent in the occluded sector of cyclones and the trowal airstream. *Mon. Wea. Rev.,* **127,** 70–88.

——, 2006: The role of shearwise and transverse quasigeostrophic vertical motions in the life cycle of the midlatitude cyclone. *Mon. Wea. Rev.,* **134,** 1174–1193.

——, J. D. Locatelli, and P. V. Hobbs, 1990: Organization and structure of clouds and precipitation on the mid-Atlantic coast of the United States. Part III: The evolution of a midtropospheric cold front. *Mon. Wea. Rev.,* **118,** 195–217.

McClain, E. P., 1960: Some effects of the western Cordillera of North America on cyclonic activity. *J. Meteor.,* **12,** 314–323.

McLay, J. G., and J. E. Martin, 2002: Surface cyclolysis in the North Pacific Ocean. Part III: Composite local energetics of tropospheric-deep cyclone decay associated with rapid surface cyclolysis. *Mon. Wea. Rev.,* **130,** 2507–2529.

Mesinger, F., and R. E. Treadon, 1995: "Horizontal" reduction of pressure to sea level: Comparison against NMC's Shuell method. *Mon. Wea. Rev.,* **123,** 59–68.

Newton, C. W., 1956: Mechanisms of circulation change in a lee cyclogenesis. *J. Meteor.,* **13,** 528–539.

Nielsen, J. W., and R. M. Dole, 1992: A survey of extratropical cyclone characteristics during GALE. *Mon. Wea. Rev.,* **120,** 1156–1167.

Oard, M. J., 1993: A method of predicting chinook winds east of the Montana Rockies. *Wea. Forecasting,* **8,** 166–180.

Palmén, E., and C. W. Newton, 1969: *Atmospheric Circulation Systems*. Academic Press, 603 pp.

Pauley, P. M., 1998: An example of uncertainty in sea level pressure reduction. *Wea. Forecasting,* **13,** 833–851.

Petterssen, S., 1956: *Weather Analysis and Forecasting.* Vol. I. McGraw-Hill, 428 pp.

Pierrehumbert, R. T., 1986: Lee cyclogenesis. *Mesoscale Meteorology and Forecasting,* P. S. Ray, Ed., Amer. Meteor. Soc., 493–515.

Price, W. B., 1971: Wind and weather regimes at Great Falls, Montana. Western Region Tech. Memo. 64, 35 pp. [Available from National Weather Service Western Region, P.O. Box 11188, Salt Lake City, UT 84147-0188.]

Reitan, C. H., 1974: Frequencies of cyclones and cyclogenesis for North America, 1951–1970. *Mon. Wea. Rev.,* **102,** 861–868.

Roebber, P. J., 1984: Statistical analysis and updated climatology of explosive cyclones. *Mon. Wea. Rev.,* **112,** 1577–1589.

——, 1989: On the statistical analysis of cyclone deepening rates. *Mon. Wea. Rev.,* **117,** 2293–2298.

Sanders, F., and J. R. Gyakum, 1980: Synoptic–dynamic climatology of the "bomb." *Mon. Wea. Rev.,* **108,** 1589–1606.

Schultz, D. M., and C. A. Doswell III, 2000: Analyzing and forecasting Rocky Mountain lee cyclogenesis often associated with strong winds. *Wea. Forecasting,* **15,** 152–173.

Schwartz, R. M., and T. W. Schmidlin, 2002: Climatology of blizzards in the conterminous United States, 1959–2000. *J. Climate,* **15,** 1765–1772.

Silberberg, S. R., 1990: The role of mesoscale features in a wintertime Great Lakes cyclone. *Wea. Forecasting,* **5,** 89–114.

Sinclair, M. R., 1994: An objective cyclone climatology for the Southern Hemisphere. *Mon. Wea. Rev.,* **122,** 2239–2256.

——, 1997: Objective identification of cyclones and their circulation intensity, and climatology. *Wea. Forecasting,* **12,** 595–612.

Smart, J. R., and F. H. Carr, 1986: Observations and analysis of a polar low over the Great Lakes region. Preprints, *11th Conf. on Weather Analysis and Forecasting,* Kansas City, MO, Amer. Meteor. Soc., 188–193.

Steenburgh, W. J., and C. F. Mass, 1994: The structure and evolution of a simulated Rocky Mountain lee trough. *Mon. Wea. Rev.,* **122,** 2740–2761.

Stewart, R. E., and Coauthors, 1995: Winter storms over Canada. *Atmos.–Ocean,* **33,** 223–247.

Tibaldi, S., A. Buzzi, and A. Speranza, 1990: Orographic cyclogenesis. *Extratropical Cyclones, The Erik Palmén Memorial Volume,* C. W. Newton and E. O. Holopainen, Eds., Amer. Meteor. Soc., 107–127.

Vinzani, P. G., and S. A. Changnon Jr., 1981: A case study: 1980's surprise long-track snowstorm. *Weatherwise,* **34** (4), 74–76.

Whittaker, L. M., and L. H. Horn, 1981: Geographical and seasonal distribution of North American cyclogenesis, 1958–1977. *Mon. Wea. Rev.,* **109,** 2312–2322.

Zishka, K. M., and P. J. Smith, 1980: The climatology of cyclones and anticyclones over North America and surrounding ocean environs for January and July, 1950–77. *Mon. Wea. Rev.,* **108,** 387–401.